CLM-P233

CLM-P233

United Kingdom Atomic Energy Authority

RESEARCH GROUP

Preprint

EXPERIMENTAL DISPERSION CURVE FOR LOW FREQUENCY DRIFT-WAVES IN AN INHOMOGENEOUS MAGNETO-PLASMA

B. E. KEEN
R. V. ALDRIDGE

Culham Laboratory
Abingdon Berkshire

1970

CONTENTS

uld be addressed to the
don, Berkshire, England

1. INTRODUCTION

During the last few years there has been considerable interest both experimentally and theoretically in the electrostatic branch of low frequency waves in an inhomogeneous magneto-plasma, in which the propagation frequency ω is much less than the ion-cyclotron frequency Ω_i. An important group of these waves are the so called 'drift' waves, whose presence necessarily depends upon the existence of some inhomogeneity in one of the equilibrium plasma parameters such as density gradient, temperature gradient, pressure gradient, or magnetic field inhomogeneity. In this paper, the case is considered in which the plasma has a constant electron temperature, and there exists a density gradient in a direction perpendicular to an axial homogeneous magnetic field. It can be shown that under certain plasma conditions the waves may be unstable with a positive growth rate, thus causing the waves to grow to large amplitudes, which are only limited by non-linear mechanisms in the plasma. At present, most of the reported experiments on drift waves have been performed on self-oscillating instabilities in various plasmas. The papers include HENDEL, CHU, and POLITZER (1968), LASHINSKY (1964), and BUCHELINIKOVA (1964). Consequently, these experiments have been performed in the non-linear regime, whereas most of the predictions have been made based on linearised theories. This paper reports propagation experiments carried out in the small amplitude, linear regime, and this allows direct comparison with some features of the linear theories. The measurements were made of the Re $(k_{\parallel})$ as the applied frequency ω was varied. Here $k_{\parallel}$ is the axial wavenumber parallel to the homogeneous magnetic field.

The simplest theory of drift waves in an inhomogeneous plasma has been considered by KADOMTSEV (1965) for a collisionless, non-rotating plasma, but this simple theory has left out several important factors that are normally encountered in any real plasma. These are (a) both the electrons and the ions suffer a large number of collisions, and, (b) that plasmas are usually moving relative to the laboratory frame because of the existence of electric fields in the bulk of the plasma and at the end electrodes. These effects can be taken into account by including in the simple theory a mean ion collision time τ_i, and a radial electric field E_r, which are the important parameters in this experimental plasma. The modified theory is developed in Section 2. Section 3 continues to describe the apparatus and the experimental techniques employed. The results obtained are discussed in Section 4, and finally, in Section 5, the results obtained are compared with the modified theory. Some of these results have been presented earlier in a short note (KEEN and ALDRIDGE 1969).

2. THEORY

The original simple theory of drift-waves (KADOMTSEV 1969) described the plasma behaviour by considering the equations of motion of the electrons and ions without collisions or electric fields included, together with the equations of continuity of each of these species. These equations were considered in the following approximations:-

(i) The 'slab' model was applied in the 'localized' approximation.

(ii) The equations were linearized to first-order for small perturbations of density n' and potential φ' in which the perturbation

was taken in the form $\exp -i(\omega t - \bar{k}.\bar{r})$, where $\bar{k}$ is the wave vector, and ω the oscillation frequency.

(iii) The inverse scale length $\kappa = \frac{1}{n_0}\left(\frac{dn_0}{dx}\right)$ was taken to be constant and in the x direction, while the uniform magnetic field B_0 was along the z direction. Propagation was considered obliquely to the magnetic field B_0, in which $k_y \gg k_x \gg \frac{1}{n_0}\left(\frac{dn_0}{dx}\right)$, where $n_0(x)$ is the equilibrium density.

(iv) The low frequency case was considered in which the propagation frequency $\omega \ll \Omega_i$, ($\Omega_i = eB/M_i c$, is the ion cyclotron frequency), in the electrostatic approximation.

(v) The non-isothermal case $T_e \gg T_i$ was considered and thus the ion pressure was neglected. Here T_e and T_i are the temperatures of the electrons and ions respectively.

The equations were solved under the conditions that the plasma was collisionless and non-rotating, and this resulted in a relationship between the frequency ω and wavenumbers k_y and $k_{||}$:-

$$\omega^2 - \omega\omega^* - k_{||}^2 c_s^2 = 0 \qquad (1)$$

where $c_s = (T_e/M_i)^{\frac{1}{2}}$ is the sound velocity, and $\omega^* = c\kappa k_y T_e/eB$. The resulting dispersion diagram is shown in Fig.1. The general features of the diagram are that it consists of two branches. The upper branch which follows a frequency shifted sound wave curve $\omega = k_{||} c_s + \omega_2$, (with $\omega_2 = \omega^*/2$), for high $k_{||}$ values, and which tends at low $k_{||}$ values (as $k_{||} \to 0$) to a cut-off frequency $\omega_1 = \omega^*$. The lower branch follows the frequency shifted sound wave curve $\omega = -k_{||} c_s + \omega^*/2$ at high $k_{||}$ values, and as $k_{||} \to 0$ it tends to a cut-off value $\omega_3 = 0$.

This picture becomes modified if the zero-order radial electric

field E_r and a mean ion collision time τ_i are included in the theory, taking account of the above approximations (i) - (v). Consider the ion equation of motion:

$$\frac{d\bar{v}_i}{dt} + \frac{\bar{v}_i}{\tau_i} = -\frac{e}{M_i}\bar{\nabla}\varphi + \frac{e}{M_i c}\left[\bar{v}_i \wedge \bar{B}_o\right] \tag{2}$$

where $\bar{v}_i$ is the ion velocity, M_i the ion mass, and where the velocity $\bar{v}_i$, density n_o, and the potential φ, are taken in the form:

$$\begin{aligned} \bar{v}_i &= \bar{v}_{io} + \bar{v}_i' \exp - i\,(\omega t - \bar{k}.\bar{r}) \\ n &= n_o + n' \exp - i\,(\omega t - \bar{k}.\bar{r}) \\ \varphi &= \varphi_o + \varphi' \exp - i\,(\omega t - \bar{k}.\bar{r}) \end{aligned} \tag{3}$$

Equating zero-order quantities in equation (2) it can be shown that:

$$x v_{io} = 0 = {}_z v_{io} \text{ and } {}_y v_{io} = \frac{-\alpha^2}{(1+\alpha^2)}\left(\frac{cE_r}{B}\right) \tag{4}$$

where $\alpha = \Omega_i \tau_i$.

By linearising equation (2) to first-order, and substituting for $\bar{v}_i'$ in the equation of continuity

$$\frac{\partial n}{\partial t} + (\bar{\nabla} . (n\,\bar{v}_i)) = 0 \tag{5}$$

an expression is obtained relating n_i' and φ', which is

$$\frac{n_i'}{n_o} = \frac{e\varphi'}{M_i\,(\omega - \omega_r)}\left[\frac{k_z^2}{\omega_1} - \frac{(k_y^2\,\omega_1 + k_y \cdot \kappa\,\Omega_i)}{(\Omega_i^2 - \omega_1^2)}\right] \tag{6}$$

where $\omega_r = k_y\, {}_y v_{io}$, and $\omega_1 = (\omega - \omega_r = i/\tau_i)$

From the electron equation of motion, it can be shown that if $k_{\parallel}$, the component of the wave vector parallel to the magnetic field, is not too small, so that the phase velocity of the wave is much smaller

than the electron thermal velocity $v_t = (T_e/m)^{\frac{1}{2}}$, the electrons follow a Boltzmann distribution so that the perturbed electron density n'_e is given by

$$\frac{n'_e}{n_o} = \frac{e\varphi'}{T_e} \tag{7}$$

In the frequency range considered, the principle of quasi-neutrality holds, and so $n'_e = n'_i$. Then, from equations (6) and (7) the following dispersion equation can be obtained:

$$W^4 - (3i/\alpha)W^3 - \left\{1 + (3/\alpha^2) + (k_y^2 + k_{||}^2)\, c_s^2/\Omega_i^2\right\} W^2$$

$$- \left\{\omega^*/\Omega_i - i\,(1+1/\alpha^2)/\alpha - 2i\,(k_y^2+k_{||}^2)\, c_s^2/\alpha\Omega_i^2\right\} W$$

$$+ k_{||}^2\, c_s^2/\Omega_i^2 + (k_{||}^2 + k_y^2)\, c_s^2/\alpha^2\Omega_i^2 + i\,\omega^*/\alpha\Omega_i = 0 \tag{8}$$

where $W = (\omega - \omega_r)/\Omega_i$.

This quartic equation is difficult to solve analytically, but in the limit that $\omega \ll \Omega_i$ it can be reduced to a quadratic equation. Then a dispersion diagram similar to Fig.1 is obtained again. This time the frequencies ω_1, ω_2 and ω_3 are given by:

$$\omega_1 = \omega_r + \alpha^2\, \omega^*/(1 + \alpha^2) \tag{9}$$

$$\omega_2 = \omega_r + \alpha^2\, \omega^*/2(\alpha^2 + 3) \tag{10}$$

$$\omega_3 = \omega_r - 2\alpha^2\, \omega^*/(\alpha^2 + 3)(\alpha^2 + 1) \tag{11}$$

The equation (8) has been solved numerically in its cubic form with the aid of a computer for the particular conditions prevailing in these experiments. The resulting curves are shown as solid lines in Figs.10 and 11 and will be discussed in Section.4.

The above calculation applied only to slab geometry but in the approximations considered it can be taken over into cylindrical geometry, such that $x \to r$, $y \to r\theta$, and $z \to z$. In this case $k_y \to m/r_o$, where m is the azimuthal mode number associated with the wave and r_o is the radius at the maximum of the wave amplitude. Also, $\omega_r = k_y\, y v_{io}$ is just the rotation of the plasma at radius r_o. Thus in Fig.1 the upper branch of the dispersion diagram is associated with the $m = +1$ mode and the lower branch with the $m = -1$ mode.

3. EXPERIMENTAL

3.1 Hollow Cathode Arc Apparatus

The hollow cathode arc apparatus is shown in Fig.2, and is essentially the same as that described by ALDRIDGE and KEEN (1970). In this particular case, the discharge was running in helium at a constant current of 20 A. The baffles or limiters shown in the diagram limit the plasma column to about 4–5 cm dia. inside the 10 cm dia. glass tube, and the experimental space was about 150 cm long. The magnetic field was uniform throughout this region to within 0.5%, and was kept constant at two values 1.00 kG and 0.75 kG, while dispersion curves were measured.

The background neutral pressure was maintained at a constant value of 2.5×10^{-4} torr throughout the experiment, by carefully varying the inflow of neutral gas through the anode, or by restricting the pumping on this region. Under these conditions the plasma proved to be fairly 'quiet' and only below 20 kHz did the 'noise' spectrum of the plasma begin to increase.

3.2 Diagnostic Techniques

Between each magnet coil were situated a set of ports, labelled (a) to (f) in Fig.2, spaced apart by 10 cm each. Each set consisted of four ports set around the azimuth, each 90^{o} apart. Interchangeable probes of various descriptions could be inserted at any of these positions. Another probe was available which could be moved longitudinally along the column, and could be set at any desired radial position. This was used either in its ion-biased state (in order to detect density oscillations) or as a floating probe. Density and temperature profiles were measured using a double probe, which could be moved radially on a micrometer carriage from the centre of the column outwards.

The rotational frequency of the arc column was determined from measurements on a single-sided ion saturation probe (BRUNDIN 1964). Previous experiments (ALDRIDGE and KEEN 1970) had shown that this technique gave results in good agreement with a suspended vane technique (BOESCHOTEN and DEMETER 1968). This single sided probe was faced into the rotation and the ion-saturation current i_s was measured and then faced away from the rotation and the difference in ion current Δi obtained. This difference was related to the rotational frequency through the expression $\omega_r = \frac{\Delta i}{r i_s}\left(\frac{T_e}{M_i}\right)^{\frac{1}{2}}$. In this way, the frequency ω_r was obtained as a function of radius r.

The radial electric field E_r is a difficult parameter to measure and various methods have been discussed in more detail by ALDRIDGE and KEEN 1970. Briefly, this electric field was obtained by three different techniques, and was deduced from:

(a) the corrected spatial variation of the floating potential φ_f.

(b) the spatial variation of plasma potential φ_p as measured using

thermionically emitting probe (KEMP and SELLEN 1966).

(c) the spatial variation of the plasma potential φ_p as deduced from the 'knee' in the log i_e versus V_a plot of a single probe curve. (Here V_a is the applied potential to the probe, and i_e is the resulting electron current drawn by the probe).

3.3 Method of wave excitation

Various method were attempted to excite density oscillations in the plasma, but the two which proved to be most successful were:

(a) four small magnetic field coils, outside the glass tube, were situated at azimuthal positions, 0, $\pi/2$, π, and $3\pi/2$, and oriented such that they produced an oscillating magnetic field $\tilde{B}_z$ in the plasma. Then, by virtue of the $[E_r \times \tilde{B}_z]$ drift an oscillating velocity $\tilde{v}_\varphi$ [or density oscillation] was produced in the plasma.

(b) four azimuthally symmetrical plates situated around the periphery of the plasma (as shown in Fig.3) were fed with an oscillating potential. This created an oscillating $\tilde{E}_r$ in the plasma, and the interaction of this with the zero order B_z, through the $[\tilde{E}_r \times \bar{B}_z]$, drift produced an oscillating ion velocity $\tilde{v}_\theta$ (or oscillating density $\tilde{n}$) in the plasma.

By correctly phasing the currents in the magnetic field coils, or the potentials to the drive plates, separate azimuthal mode numbers of $m = 0, +1$ or -1 could be selected. Ultimately, most of the results were obtained with the method (b) as this proved to be more efficient at lower frequencies, and also at the shorter wavelengths. The plates were radially moveable, but were normally kept at a constant equal radii in the range $r = 1.8 - 2.0$ cm. They were constructed

from tungsten plate and were 0.5 cm long in the axial direction and 1.2 cm in the azimuthal direction.

The electronic set-up is shown in Fig.3. It is seen that the oscillator set at a frequency f in the range 20-220 kHz, was transformer coupled to a system of four power amplifiers, which individually feed one plate in the plasma. The phase shifter shown in one lead to the power amplifiers allowed the phase to be shifted by $+ \pi/2$ or $- \pi/2$, whereas the output from each power amplifier could be chosen so that its phase was in-phase with the input, or shifted by π. Consequently, by arranging these phases correctly, the separate azimuthal modes $m = 0, + 1, m - 1$ could be chosen. The wave signal in the plasma was detected on the ion-biased longitudinally moving probe which was motor driven along the length of the plasma. This signal was coupled into a low noise amplifier, and then through a narrow band filter (set at f), into the 'signal' channel of a phase sensitive detector (P.S.D.). The 'reference' channel of the P.S.D. was fed from the main oscillator through another phase shifter. The output of the P.S.D. (proportional to $A \cos (k_{\parallel} z)$, where A is the amplitude of the wave) was fed into the Y input of an $X - Y$ recorder. The X arm was fed with a voltage proportional to the longitudinal position of the detection probe. Typical output plots are shown in Fig.4, taken at $f = 170$ kHz for both the $m = + 1$ and $m = - 1$ modes. From these plots the axial wavelength, and consequently $k_{\parallel}$, could be obtained as a function of frequency, thus allowing a $(\omega - k_{\parallel})$ dispersion diagram to be constructed for each separate mode number.

4. RESULTS

4.1 DC Properties

The density and temperature profiles of the plasma were obtained using the double probe technique (JOHNSON and MALTER 1950). The results obtained in the magnetic fields $H = 0.75$ kG and $H = 1.00$ kG are shown in Figs.5(a) and (b). The basic features of these curves are a peak density of 2.0×10^{12} cm^{-3} with a constant inverse scale length $\kappa = \frac{1}{n_o}\left(\frac{dn_o}{dr}\right) \approx 0.65 \pm 0.05$ cm^{-1} within a radius range 0.6-3.0 cm, and a constant electron temperature $T_e = 7.0 \pm 0.3$ eV within a 3.5 cm dia.

The results of the plasma rotational frequency as a function of radius measured with the one-sided probe are shown in Fig.6(a) for $H = 0.75$ kG and in Fig.6(b) for $H = 1.00$ kG. It is seen that frequency values of 16 ± 3 kHz at 0.75 kG and 20 ± 4 kHz at 1.00 kG within the radius range 0.5 - 1.5 cm are obtained.

The plasma potential φ_p as a function of radius is shown in Fig.7. These results were obtained from the 'knee' in the single Langmuir probe plot of log i_e versus the applied voltage V_a. Essentially, similar results were obtained with the thermionically emitting probe, although less reliable results were achieved with this technique. It is seen that a reasonably constant radial electric field $E_r \left(= \frac{\partial \varphi_p}{\partial r}\right)$ is obtained, which is (a) - 2.1 ± 0.3 volts/cm at $H = 0.75$ kG and, (b) - 2.8 ± 0.4 volts/cm at $H = 1.00$ kG.

The parameter α $(= \Omega_i \tau_i)$ was found by substituting the appropriate values of E_r and ω_r in equation (4) namely, $\omega_r = \alpha^2 \, cE_r/r_o \, H(1+\alpha^2)$. This resulted in a value of $\alpha = 0.87 \pm 0.07$ at $H = 1.00$ kG, and $\alpha = 0.73 \pm 0.07$ at $H = 0.75$ kG.

4.2 AC Properties

When a density wave was propagating in the plasma it was checked at various axial positions so that the excited mode was consistent along the column. Fig.8 shows typical results obtained at a point 20 cm from the exciting system for azimuthal phase measurements in (a) the $m = -1$ mode and (b) the $m = +1$ mode, at an excitation frequency of 100 kHz. These results were obtained by using a fixed detecting probe and rotating the magnetic coil excitation system outside the tube. Fig.8(c) shows the amplitude measurements which were obtained simultaneously. It is seen that the phase changes linearly with azimuthal angle consistent with (a) a $m = -1$, and (b) a $m = +1$ propagating azimuthal mode. The radial variation of (a) $|A| \cos \varphi$, and, (b) the radial phase angle φ are shown in Fig.9, and, again, it is seen that this is consistent with an $m = |1|$ propagating mode in the plasma. Throughout most of the experiments the density perturbation (n') was not allowed to reach a value of $n'/n_0 > 1\%$.

The wavelengths $\lambda_{\parallel}$ corresponding to each frequency were determined directly from traces such as those shown in Fig.4. In principle, it should be possible to obtain values for the attenuation coefficient of the wave as a function of frequency, but as the frequency was reduced the efficiency of wave production reduced correspondingly. Also, the wavelength became longer and began to approach the length of the apparatus at the lowest frequencies. This meant that reliable data on the decay of the wave were impossible to obtain, and also wavelength values were subject to fairly large percentage errors, as can be seen from the experimental dispersion diagrams. The resulting dispersion diagrams are shown in Fig.10 for $H = 1.00$ kG and in Fig.11 for $H = 0.75$ kG. Considering Fig.10, it is seen, typically, that

both the $m = +1$ and $m = -1$ mode waves appear to satisfy a linear (ω, k) relationship for larger $k_{\parallel}$ values, and that as $k_{\parallel} \rightarrow 0$ both modes appear to tend towards cut-off frequencies. However, the $m = 0$ mode wave seems to obey a linear relationship without deviation, right down to 20 kHz. The corresponding slope of this line results in a phase velocity of $1.20 \pm 0.15 \times 10^6$ cm/sec, compared with a predicted theoretical ion sound velocity, $c_s = (T_e/M_i)^{\frac{1}{2}}$ of $1.28 \pm 0.04 \times 10^6$ cm/sec. In Figs.10 and 11 the full curve is that obtained from solving numerically, on a computer, the cubic part of the theoretical dispersion curve, (equation (8)), using the appropriate values for the physical parameters. It is seen that reasonable agreement with theory is obtained. Table 1 summarises the various cut-off frequencies and phase velocities predicted by theory compared with the experimental value. Here again, it is seen that reasonable agreement with the theory is achieved.

5. DISCUSSION AND CONCLUSION

In order to compare the experimental results with theoretical predictions, it has been necessary to extend the simple theory of KADOMTSEV (1965) in order to include the effects of a radial electric field, and a finite ion collision time τ_i. One of the problems of making a comparison is that the theoretical calculation has been performed in cartesian or 'slab' geometry, whereas the experimental results are for a cylindrical plasma. In the calculation the cylindrical case has been approximated by taking over the 'slab' situation such that $x \rightarrow r$, $y \rightarrow r\theta$, and $z \rightarrow z$. As a consequence $k_y \rightarrow m/r_o$, where m is the azimuthal mode number, and r_o has been taken as the radius at which there was a maximum in the wave amplitude. Also,

TABLE 1

Parameter	Theory H = 1 kG	Experiment H = 1 kG	Theory H = 0.75 kG	Experiment H = 0.75 kG
m = + 1 Cut-off frequency (ω_1)	67±10 kHz	60±10 kHz	66±10 kHz	55±10 kHz
m = - 1 Cut-off frequency (ω_3)	-7± 5 kHz	-20±10 kHz	-13±7 kHz	-25±10 kHz
Slope of m = 0 line (c_s)	$1.28\pm.04 \times 10^6$ cm/sec	$1.20\pm.15 \times 10^6$ cm/sec	$1.28\pm.04 \times 10^6$ cm/sec	$1.20\pm.15 \times 10^6$ cm/sec

$k_y\, y v_{oi} \rightarrow m_y v_{io}/r_o = m\,\omega_r$, which is the rotation of the column at the radius r_o. Hence, in order to compare these calculations with the cylindrical experimental case, it is necessary to assume that the azimuthal wave vector k_y should be large compared with the inverse radial scale length κ, (i.e. $r_o\,\kappa \ll 1$). In fact in this case $r_o\,\kappa \approx 0.5$, and this is an important point of divergence.

Another important point is that the 'slab' model used is based on the 'local' approximation (i.e. $k_y \gg k_x$). A much more realistic calculation would be to set up the appropriate differential equation for potential φ or density n perturbation from the equations of motion. This could, then, be solved with the appropriate boundary conditions taken into account. The solutions to the eigenvalue problem could then be used to obtain the dispersion diagram in the cylindrical case. Therefore, the neglect of the x dependence in the calculation, can only be justified if $r_o\,\kappa \ll 1$ (i.e. the weakly inhomogeneous case). As pointed out, experimentally, this condition is not completely justified.

The theory has been considered in the low frequency approximation ($\omega/\Omega_i \ll 1$), and at the low frequencies as $k_{||} \to 0$, this is well satisfied. Consequently, the cut-off frequencies ω_1 and ω_3 have been obtained by solving the dispersion equation (8), including only terms up to those quadratic in $W[= (\omega - \omega_r)/\Omega_i]$. At higher frequencies, for finite $k_{||}$, this equation was solved numerically including cubic terms in W. The resulting curves are shown as the full line in Figs.10 and 11 solved under the appropriate conditions. The portion between $1/\lambda_{||} = 0.06 \to 0.10$ has been dotted since two roots of the cubic equation cross in this region, one the root shown and another highly damped root, which would not show up experimentally.

Experimentally, the small amplitude, low frequency approximation was justified throughout most of the range, except at the highest frequencies where ω/Ω_i approached 0.5. It was found possible to obtain results for the dispersion curve, only for ω against the $\mathrm{Re}(k_{||})$, since reliable results for the damping rate could not be obtained for the reasons stated in Section 4. Hence, in view of the difficulties associated with the theory, and the errors in the experimental results the agreement between the results and theory is reasonable.

ACKNOWLEDGEMENTS

The authors would like to acknowledge the skilful assistance of N.R.G. Ainsworth and W.H.W. Fletcher in performing the experiments, and G.N. Harding and C.N. Lashmore-Davies for many helpful discussions.

REFERENCES

ALDRIDGE, R.V. and KEEN, B.E. (1970) Plasma Phys. 12, 1.

BOESCHOTEN, F. and DEMETER, L.J. (1968) Plasma Phys. 10, 391.

BRUNDIN, C.L. (1964) University of Calif., Berkeley. Rep. A 5-64-9.

BUCHELINKOVA, N.S. (1964) Zh. Eksp. Teor. Fiz. 46, 1147, (Soviet Phys. J.E.T.P. 19, 773).

HENDEL, H.W., CHU, T.K. and POLITZER, P.A. (1968) Phys. Fluids, 11, 2426.

JOHNSON, E.O. and MALTER, L. (1950) Phys. Rev. 80, 58.

KADOMTSEV, B.B. (1965) Plasma Turbulence, Academic Press, N.Y.

KEEN, B.E. and ALDRIDGE, R.V. (1969) Phys. Lett. 29A, 575.

KEMP, R.F. and SELLEN, J.M. (1966) Rev. Sci. Instrum. 37, 55.

LASHINSKY, H. (1964) Phys. Rev. Letters 12, 121.

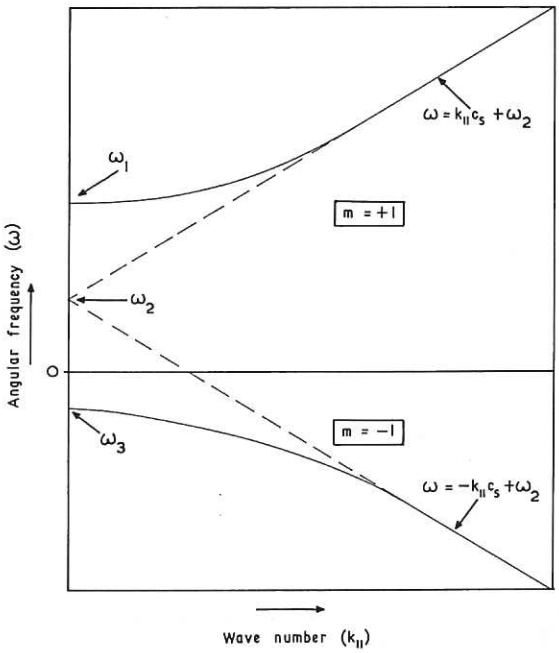

Fig.1 Dispersion diagram for drift-waves in a magnetic-plasma.

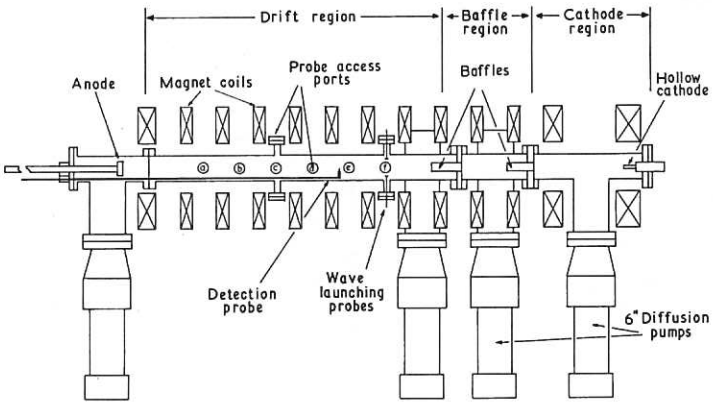

Fig.2 Schematic diagram of hollow-cathode arc apparatus.

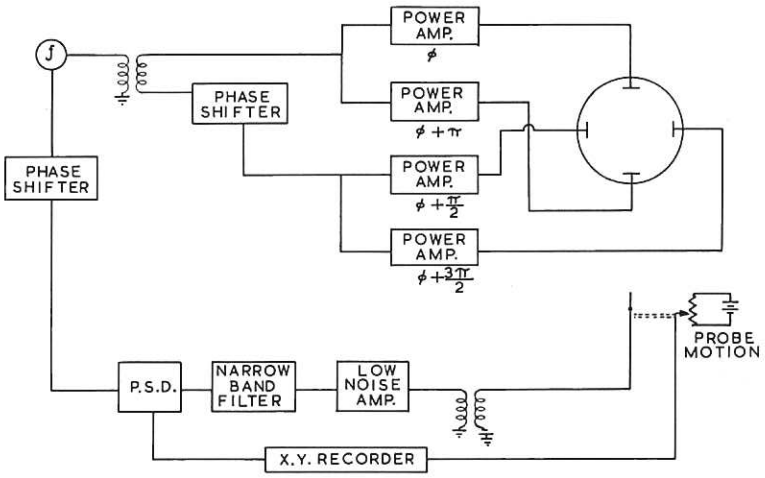

Fig.3 Schematic diagram of electronic apparatus. CLM-P233

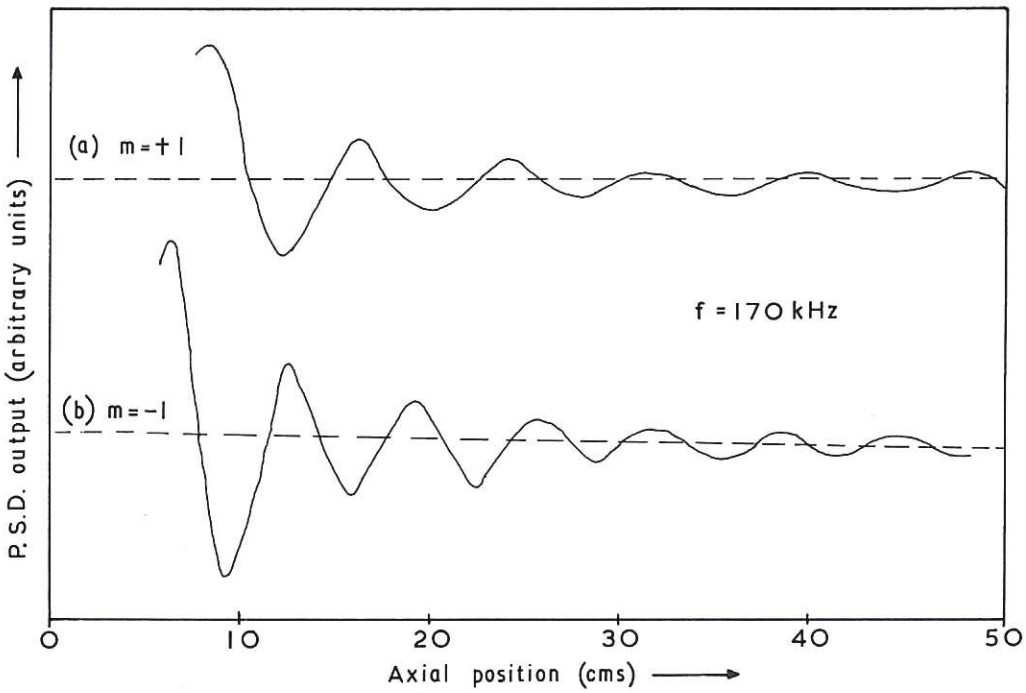

Fig.4 X-Y recorder output showing the amplitude A cos k z as a function of longitudinal position z at f = 170 kHz for (a) m = + 1 and (b) m = − 1 mode number.

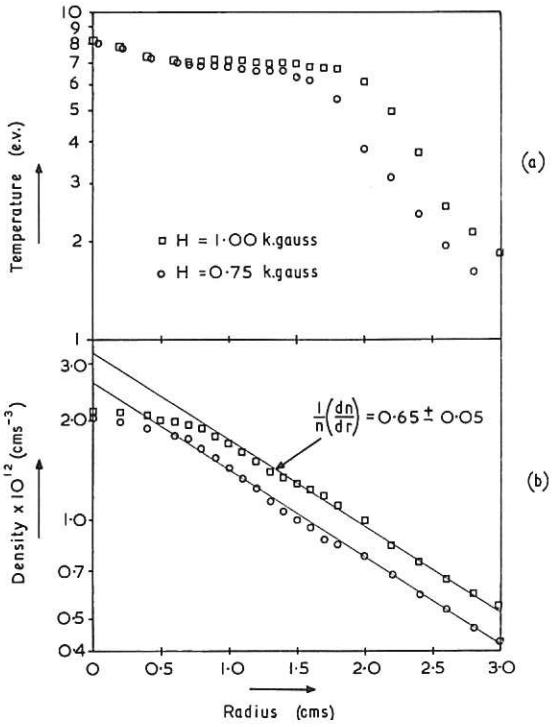

Fig.5 The density and temperature profiles taken in the magnetic fields of 1.00kG and 0.75kG.

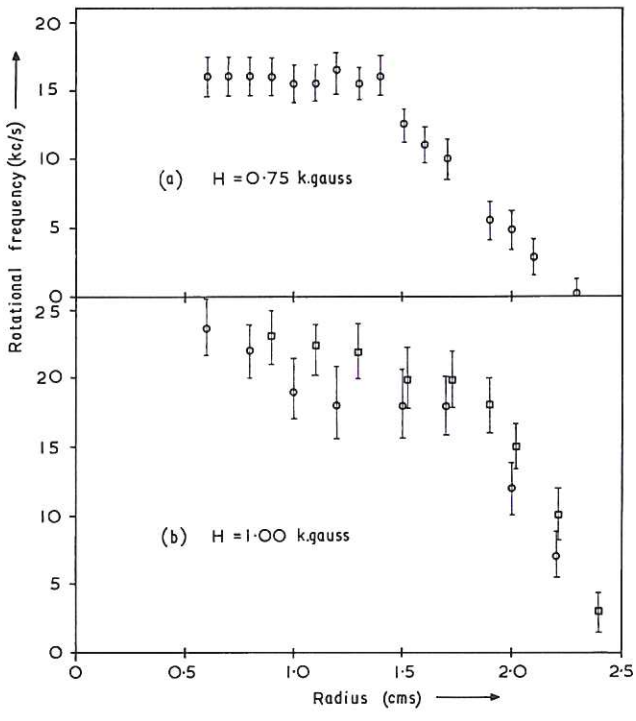

Fig.6 The measured rotational frequency ω_r as a function of radius r at (a) H = 0.75 kG and (b) H = 1.00 kG.

CLM-P233

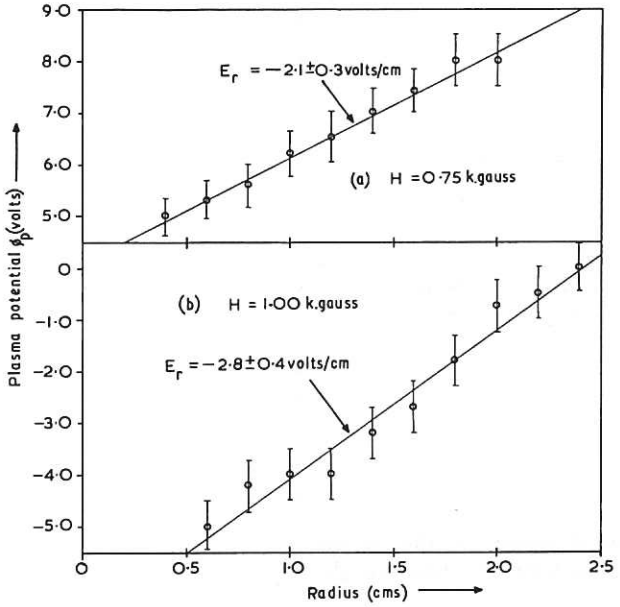

Fig.7 The measured plasma potential ϕ_p as a function of radius r at (a) H = 0.75 kG and (b) H = 1.00 kG.

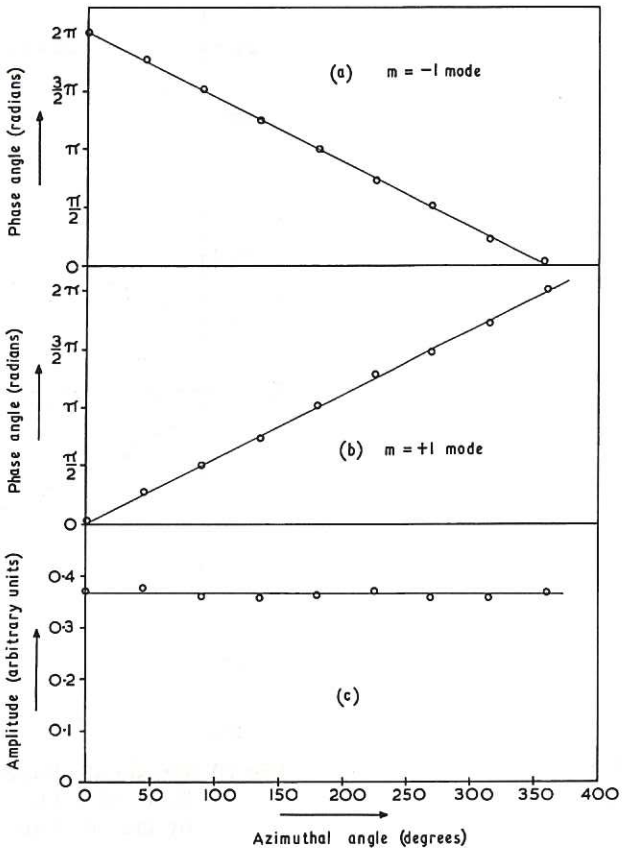

Fig.8 (a) Phase angle variation for m = − 1, (b) Phase angle variation for m = + 1 and (c) amplitude, as a function of the azimuthal angle.

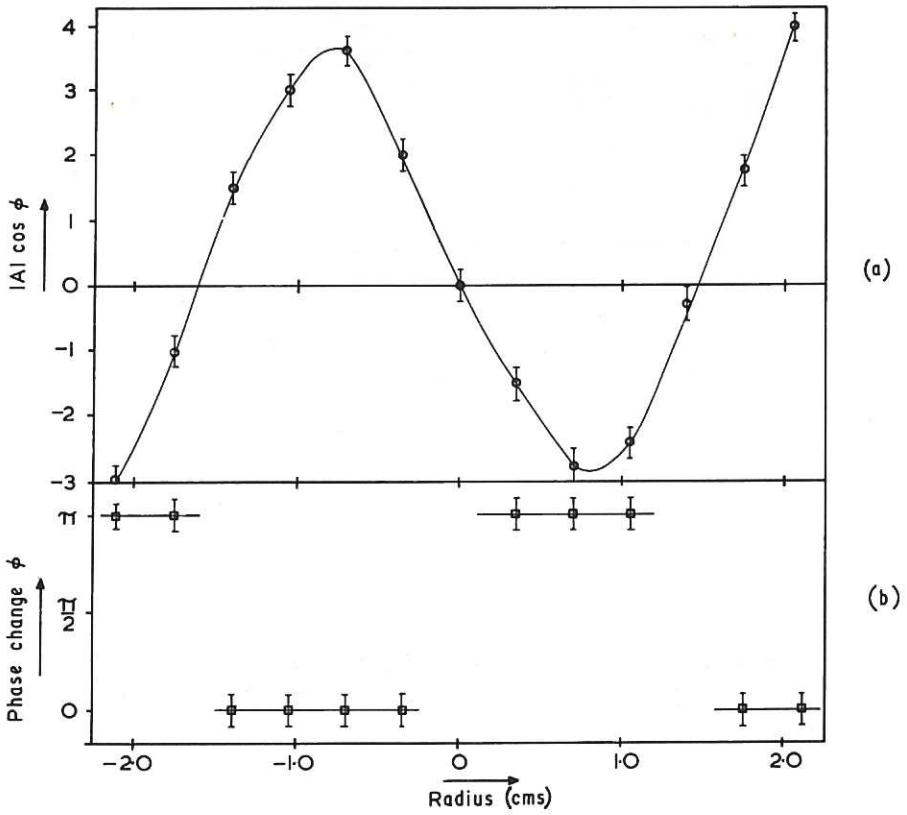

Fig.9 (a) The output of the P.S.D. proportional to |A| cos ψ, and (b) the phase change ψ, as a function of radial position (r).

CLM-P 233

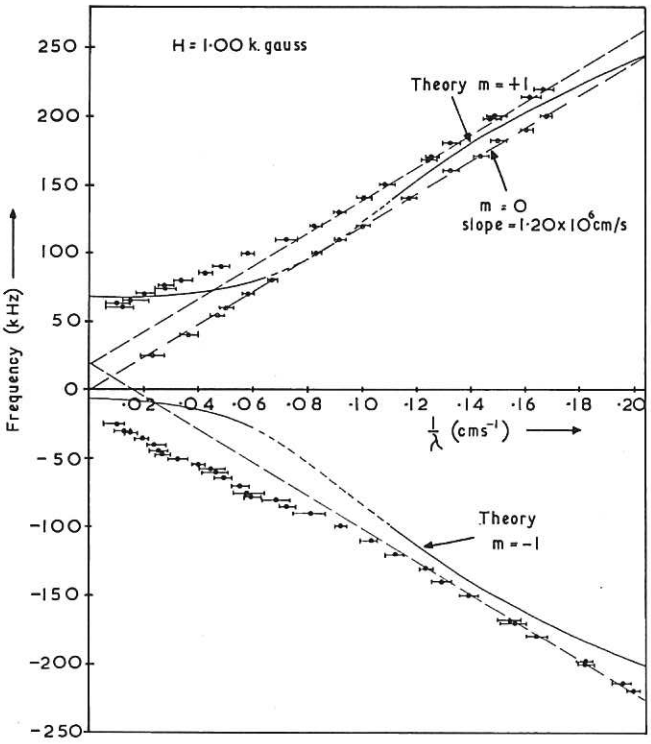

Fig.10 Measured dispersion diagram at the magnetic field of 1 kG. The theoretical curve is shown by the full line.

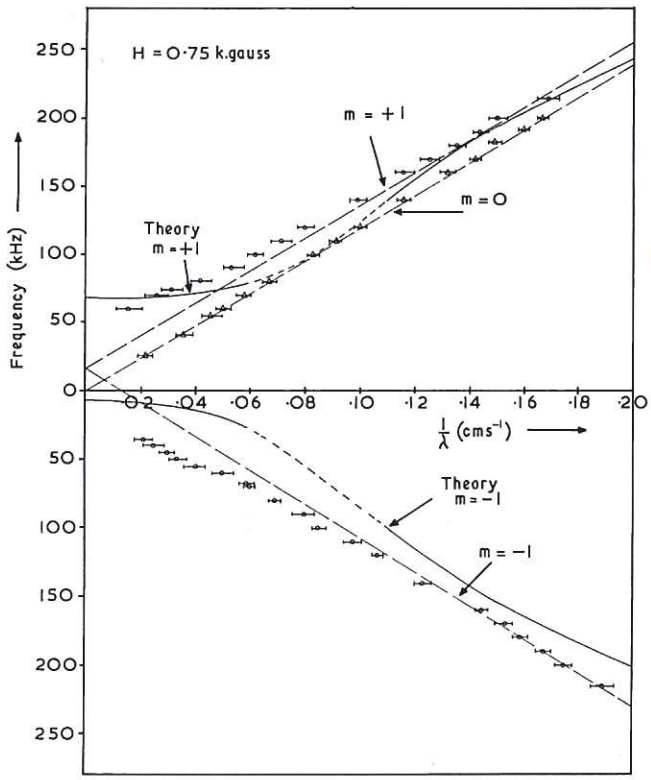

Fig.11 Measured dispersion diagram at the magnetic field of 0.75 kG. The theoretical curve is shown by the full line.